optics

MDPI

Article

A Theoretical Description of Node-Aligned Resonant Waveguide Gratings

Maik Meudt [1,2], Andreas Henkel [1,2], Maximilian Buchmüller [1,2] and Patrick Görrn [1,2,*]

[1] Chair of Large Area Optoelectronics, University of Wuppertal, Rainer-Gruenter-Str. 21, 42119 Wuppertal, Germany; mmeudt@uni-wuppertal.de (M.M.); henkel@uni-wuppertal.de (A.H.); buchmueller@uni-wuppertal.de (M.B.)
[2] Wuppertal Center for Smart Materials & Systems, University of Wuppertal, Rainer-Gruenter-Str. 21, 42119 Wuppertal, Germany
* Correspondence: goerrn@uni-wuppertal.de; Tel.: +49-202-439-1424

Abstract: Waveguide gratings are used for applications such as guided-mode resonance filters and fiber-to-chip couplers. A waveguide grating typically consists of a stack of a single-mode slab waveguide and a grating. The filling factor of the grating with respect to the mode intensity profile can be altered via changing the waveguide's refractive index. As a result, the propagation length of the mode is slightly sensitive to refractive index changes. Here, we theoretically investigate whether this sensitivity can be increased by using alternative waveguide grating geometries. Using rigorous coupled-wave analysis (RCWA), the filling factors of the modes of waveguide gratings supporting more than one mode are simulated. It is observed that both long propagation lengths and large sensitivities with respect to refractive index changes can be achieved by using the intensity nodes of higher-order modes.

Keywords: waveguide gratings; guided modes; sensitivity; propagation length; symmetry

Citation: Meudt, M.; Henkel, A.; Buchmüller, M.; Görrn, P. A Theoretical Description of Node-Aligned Resonant Waveguide Gratings. *Optics* **2022**, *3*, 60–69. https://doi.org/10.3390/opt3010008

Academic Editor: Ángel S. Sanz

Received: 27 January 2022
Accepted: 3 March 2022
Published: 4 March 2022

1. Introduction

Passive and low-loss planar optical waveguides can transport light over large areas [1–4]. When they are combined with optical elements such as diffraction gratings (termed waveguide gratings), they can be used for applications such as optical filters [5–10] and sensors [11–17] via exploiting guided mode resonances. Commonly, only the spectral positions of resonance are sensitive to refractive index changes, while the corresponding propagation length L_{prop} remains almost constant. This circumstance indicates the necessity of spectrometers for such devices based on waveguide gratings. With a large sensitivity of L_{prop}, small refractive index changes could be directly translated into a spatial variation in the outcoupled guided light. This can be detected by an array of simple broadband photodetectors.

Beyond passive refractive index sensors, a large sensitivity would allow for electrical control of L_{prop}, which opens up new possibilities such as active beam deflectors or modulators. To meet the requirement of long propagation lengths, it is desirable to use fast and loss-free effects such as the electro-optic Pockels or Kerr effect. However, those effects enable small refractive index tuning in the order of $\Delta n \approx 10^{-4} \ldots 10^{-3}$ [18–20] only, which requires large sensitivities of L_{prop}. Thus, it is of no surprise that reports about electrooptic detuning of waveguide gratings can only rarely be found in the literature to date and rather show the control of the spectral positions of resonances than the control of the propagation length [21,22].

In fact, there is a way to overcome these limits. It has been shown that intensity nodes of TE modes (s-polarized modes with a transversal electric field node) can be used to maximize the propagation length [23–25] by placing a lossy, diffractive, or scattering structure at the node position. This way, spectrally narrow resonances can also be obtained [26]. Conceptually, it has been estimated that such node modes should provide high sensitivities, as a slight shift of the node position largely affects the propagation length [27]. However, this concept has not been discussed in the scientific literature yet.

Here, we explicitly and exemplarily show that the node of the TE_1 mode in planar waveguide gratings allows obtaining long propagation lengths of more than $10^5\lambda$ and large sensitivities in the order of $L_{prop}(n)/L_{prop}(n+\Delta n) \approx 1.5 \times 10^6$ for $\Delta n = 1 \times 10^{-4}$.

2. Results and Discussion

2.1. Definition of Geometry and Symmetry Parameters

A visualization of the sensitivity of the propagation length with respect to refractive index changes is shown in Figure 1a,b. Light propagates through a waveguide grating mode in the positive x-direction. Due to the interaction with the grating, light is emitted into free space with a propagation length L_{prop} under a mean angle θ_0 and with an angular divergence of $\Delta\theta$. Without a change in the refractive index, the propagation length is large, and $\Delta\theta$ is small. When a refractive index change Δn is introduced, the propagation length is much shorter, and $\Delta\theta$ is larger. Detailed equations on these relations are provided later in this text.

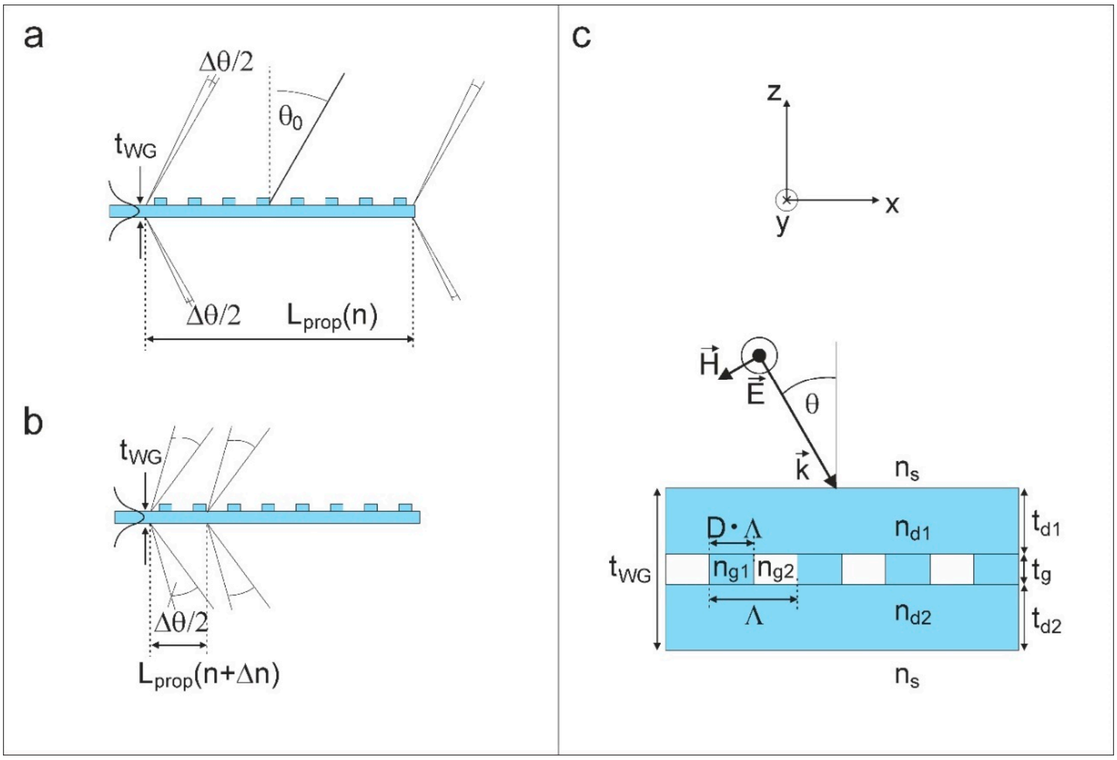

Figure 1. (**a**) A waveguide grating with an eigenmode of large propagation length L_{prop} and, thus, a small angular divergence $\Delta\theta$. θ_0 is the mean angle under which light is emitted; (**b**) a shorter propagation length L_{prop} and larger $\Delta\theta$ under refractive index tuning ($n \rightarrow n + \Delta n$); (**c**) the definition of the geometry parameters of the proposed waveguide grating. TE-polarized light is considered. Further details are provided in the text.

To present a strategy for how a large sensitivity of the propagation length can be achieved, we used the geometry of a waveguide grating, which is defined by the parameters in Figure 1c. It consists of an infinitely extended rectangular grating of period Λ, refractive indices n_{g1} and n_{g2}, and a duty cycle D. Two dielectric layers of thicknesses t_{d1} and t_{d2}, as well as refractive indices n_{d1} and n_{d2}, surround the grating. For all simulations in this research, we considered s-polarized plane-wave incidence (TE) in the x–z plane, with a lateral momentum $k_{x,0}$.

To provide a measure of symmetry for both the waveguide grating's refractive indices and thicknesses, we defined the symmetry parameters as

$$\chi_{gp} = 1 - \frac{|t_{d1} - t_{d2}|}{t_{d1} + t_{d2}}$$

and

$$\chi_n = \frac{n_{d1}}{n_{d2}},$$

where "*gp*" represents the grating position, and "*n*" represents the refractive index profile. Values of $\chi_{gp} = 1.0$ and $\chi_n = 1.0$ indicate a fully symmetric waveguide grating.

2.2. Geometry with $n_{g1} = n_{g2}$

To introduce some measures of interest and explain the role of the TE_k mode, as well as the role of symmetry, we defined a waveguide grating with the parameters $t_d = 0.632\ \lambda$, $t_g = 0.079\ \lambda$, $n_s = 1.0$, $n_{d1} = n_{d2} = 1.5$ ($\chi_n = 1.0$), and $n_{g1} = n_{g2} = 1.275$, and compared the cases of $\chi_{gp} = 0.0$ (Figure 2a,b) and $\chi_{gp} = 1.0$ (Figure 2c,d). As it is known from the literature, such a waveguide grating exhibits eigenmodes (TE_k) that can be found for distinct real-valued lateral momenta $k_{x,0,k} = k_0\ n_{eff,TE,k}$, whereby $n_{eff,TE,k}$ is the effective refractive index of an eigenmode. The index k counts the number of nodes of the electric field distribution $Re(E_y)$ attributed to an eigenmode. Thus, the TE_0 has no nodes of $Re(E_y)$, while the TE_1 mode exhibits exactly one node of $Re(E_y)$. This node causes an interesting behavior of the filling factor of the grating layer

$$FF = \frac{\int_{z_g}^{z_g+t_g} |E_y|^2 dz}{\int_{-\infty}^{\infty} |E_y|^2 dz},$$

where z_g and $z_g + t_g$ define the first and second interface of the grating layer with respect to z. While relatively large values of FF between 0.033 and 0.129 occur for all asymmetric cases as well as for the TE_0 mode at $\chi_{gp} = 1.0$, we observe a substantially lower value of $FF = 0.002$ for the TE_1 mode when $\chi_{gp} = 1.0$.

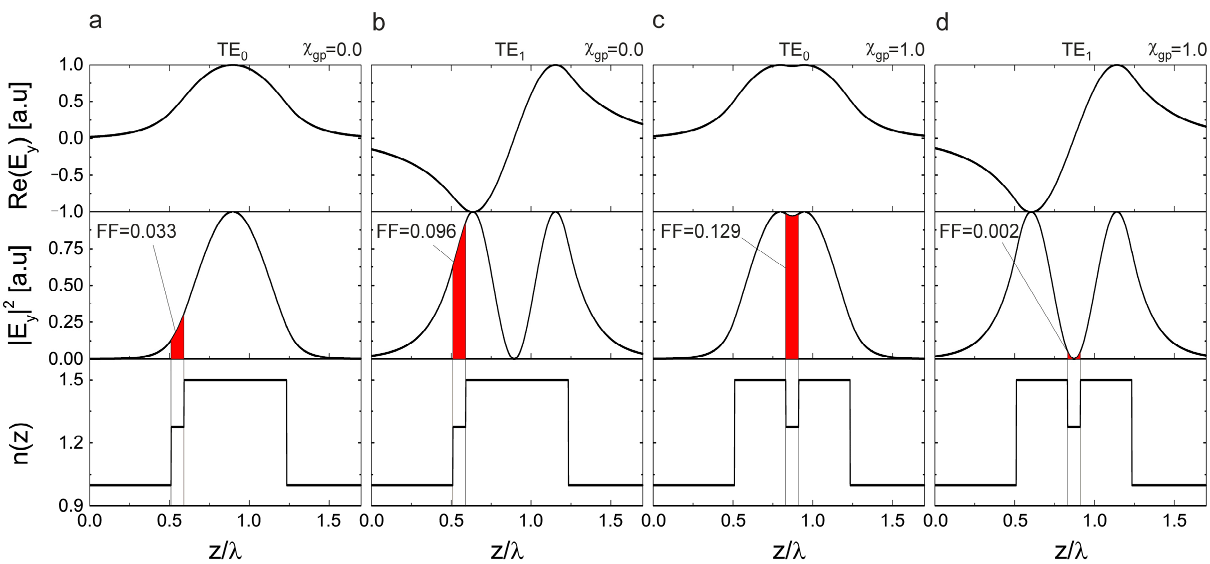

Figure 2. The distributions of the normalized electric field $Re(E_y)$ and normalized intensity $I \propto |E_y|^2$ as well as filling factors (FF) of two exemplary waveguide grating geometries with $t_{d1} + t_{d2} = 0.632\ \lambda$, $t_g = 0.079\ \lambda$, $n_s = 1.0$, $n_{d1} = n_{d2} = 1.5$ ($\chi_n = 1.0$) and $n_{g1} = n_{g2} = 1.275$: (**a**) TE_0 mode at $\chi_{gp} = 0$; (**b**) TE_1 mode at $\chi_{gp} = 0.0$; (**c**) TE_1 mode at $\chi_{gp} = 1.0$; (**d**) TE_1 mode at $\chi_{gp} = 1.0$.

2.3. Geometry with $n_{g1} \neq n_{g2}$ with Variation in Symmetry Parameters

The grating ($t_g > 0$, $n_{g1} \neq n_{g2}$) acts as a discrete lateral momentum reservoir providing a set of lateral momenta $k_{m,k} = k_{x,0,k} + m\frac{2\pi}{\Lambda}$ as a result of Floquet's theorem [28]. The physical consequence of this set of momenta is that a mode of initial lateral momentum $|\frac{Re(k_{m,k})}{k_0}| > n_s$ couples to free-space modes for $|\frac{Re(k_{m,k})}{k_0}| < n_s$. As a result, the initially real-valued $n_{eff,TE,k}$ becomes complex-valued. The intensity of an excited mode dampens to 1/e of its initial value by radiation over the normalized propagation length $\frac{L_{prop}}{\lambda} = \frac{1}{4\pi\ Im(n_{eff,TE,k})}$ due to radiation into free-space modes. Radiated light enters the free space under an angle of $\theta_0 = \arcsin(\frac{Re(k_{m,k})}{n_s\ k_0})$ and angular divergence of the diffracted light of $\Delta\theta = \frac{2Im(n_{eff,TE,k})}{n_s\ cos(\theta_0)}$. Here, we chose $n_{g1} = 1.0$, $n_{g2} = 1.5$, $D = 0.5$ with otherwise identical parameters as for the waveguide grating discussed in Figure 2. Figure 3a,b show L_{prop} and $\Delta\theta$ as functions of χ_{gp} with fixed values of $t_{d1} + t_{d2} = 0.632\ \lambda$, $\Lambda = 0.632\ \lambda$, and $t_g = 0.079\ \lambda$ (the grating position is shifted through a waveguide grating of fixed thickness). For $\chi_{gp} = 0.0$, we obtained small values of $\frac{L_{prop}}{\lambda}$ of around 10^2 and large values of $\Delta\theta$ of around $0.1°$, for both the TE_0 and the TE_1 mode. Strikingly, for $\chi_{gp} = 1.0$, the TE_1 mode exhibits large values of $\frac{L_{prop}}{\lambda} = 1.2 \times 10^5$ and small values of the divergence angle around $\Delta\theta = (10^{-4})°$. The distributions of $Re(E_y)$ and $|E_y|^2$ in Figure 3c–e for the TE_0 and TE_1 mode at $\chi_{gp} = 0.0$, as well as for the TE_0 mode at $\chi_{gp} = 1.0$, are spatially distorted in comparison to the corresponding ones in Figure 2. Such distortions can be understood as radiation sources and indicate that the grating strongly couples guided waves to radiating waves. For the TE_1 mode at $\chi_{gp} = 1.0$ (Figure 3f), almost no such distortion can be observed.

This behavior of $\frac{L_{prop}}{\lambda}$, $\Delta\theta$, and the field distributions originates from the small value of FF discussed in Figure 2: empirically, for thin gratings ($t_g < 0.1\ t_{WG}$), we find the relation

$$\frac{L_{prop}}{\lambda} \propto \frac{1}{t_g^p}$$

We observed that the TE_1 mode at $\chi_{gp} = 1.0$ exhibits $p = 6$, and thus, $\frac{L_{prop}}{\lambda} \propto= t_g^{-6}$. In comparison, the TE_0 mode at $\chi_{gp} = 1.0$ and $\chi_{gp} = 0.0$ as well as the TE_1 mode at $\chi_{gp} = 0.0$ show $p = 2$. These dependencies presumably occur because the radiative loss rate α of the grating scales with $\alpha \propto t_g^2$ and the filling factor approximately scales with $FF \propto t_g^3$ and $FF \propto t_g^1$, respectively. As a side note, gratings with dominant Ohmic losses (e.g., metallic gratings) show scalings of $p = 3$ (TE_1 mode, $\chi_{gp} = 1.0$) and $p = 1$ for all other cases.

Figure 4a,b show L_{prop}/λ and $\Delta\theta$ with variation in t_g/λ at a fixed value of $t_{d1} + t_{d2} = 0.632\ \lambda$. Decreasing values of t_g/λ lead to increasing values of L_{prop}/λ and decreasing values of $\Delta\theta$ with the explained proportionalities. These trends can be observed up to a value of $t_g = 0.4\ \lambda$, corresponding to $\frac{t_g}{t_{WG}} \approx 0.39$.

Figure 4c,d show L_{prop}/λ and $\Delta\theta$ with variation in t_{WG}/λ at a fixed value of $t_g = 0.079\ \lambda$. L_{prop}/λ is strongly increased for the TE_1 mode at $\chi_{gp} = 1.0$ in comparison to all other displayed cases for all values of t_{WG}/λ above the cutoff of the TE_1 mode.

Thus, as long as t_g is small, compared with t_{WG}, and t_{WG} is large enough to support the TE_1 mode, its increased values of L_{prop}/λ and decreased values of $\Delta\theta$ can be obtained over a broad range of waveguide grating thicknesses in the case of $\chi_{gp} = 1.0$ and $\chi_n = 1.0$.

To present an impression of the meaning of these values in an optical application, we considered the TE_1 mode and $\chi_{gp} = 1.0$ for a wavelength of $\lambda = 632.8$ nm with a grating thickness of $t_g = 0.079\ \lambda = 50$ nm. For these values, we obtained $L_{prop} = 7.6$ cm. In comparison, the standard scenario of a TE_0 mode and $\chi_{gp} = 0.0$ leads to $L_{prop} = 110$ µm. To reach the same L_{prop} as for the TE_1 mode at $\chi_{gp} = 1.0$, the grating thickness would have to be reduced to 0.88 nm (a factor of 1/56) or the waveguide grating thickness (for $t_g = 50$ nm) would have to be increased to approximately $t_{WG} = 7$ µm (a factor of 15).

Therefore, for a given grating geometry and waveguide grating thickness, using the TE_1 mode at $\chi_{gp} = 1.0$ allows for a drastic increase in the propagation length in comparison to standard waveguide gratings using the TE_0 mode.

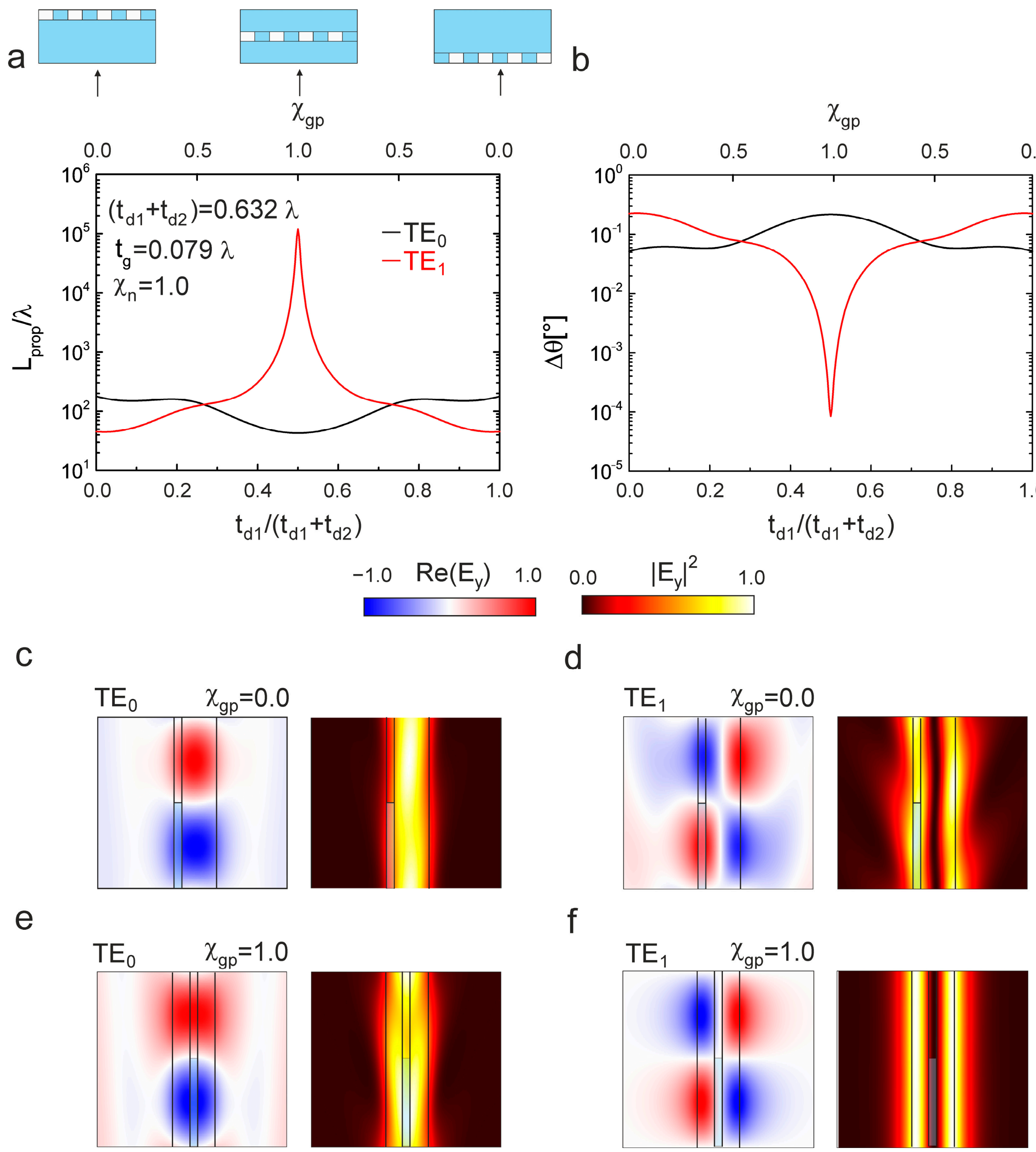

Figure 3. Variation in the asymmetry parameter χ_{gp} of a waveguide grating with $n_{g1} = 1.0$, $n_{g2} = 1.5$ and $D = 0.5$ under a constant value of $t_{d1} + t_{d2} = t_d = 0.632\ \lambda$. All other parameters are identical to the ones discussed in Figure 2: (**a**) the normalized propagation length L_{prop}/λ and (**b**) the divergence angle of the TE_0 mode (black) and TE_1 mode (red); (**c**–**f**) normalized electric fields $Re(E_y)$ and intensities $I \propto |E_y|^2$ of the TE_0 mode and TE_1 mode for $\chi_{gp} = 0.0$ and $\chi_{gp} = 1.0$.

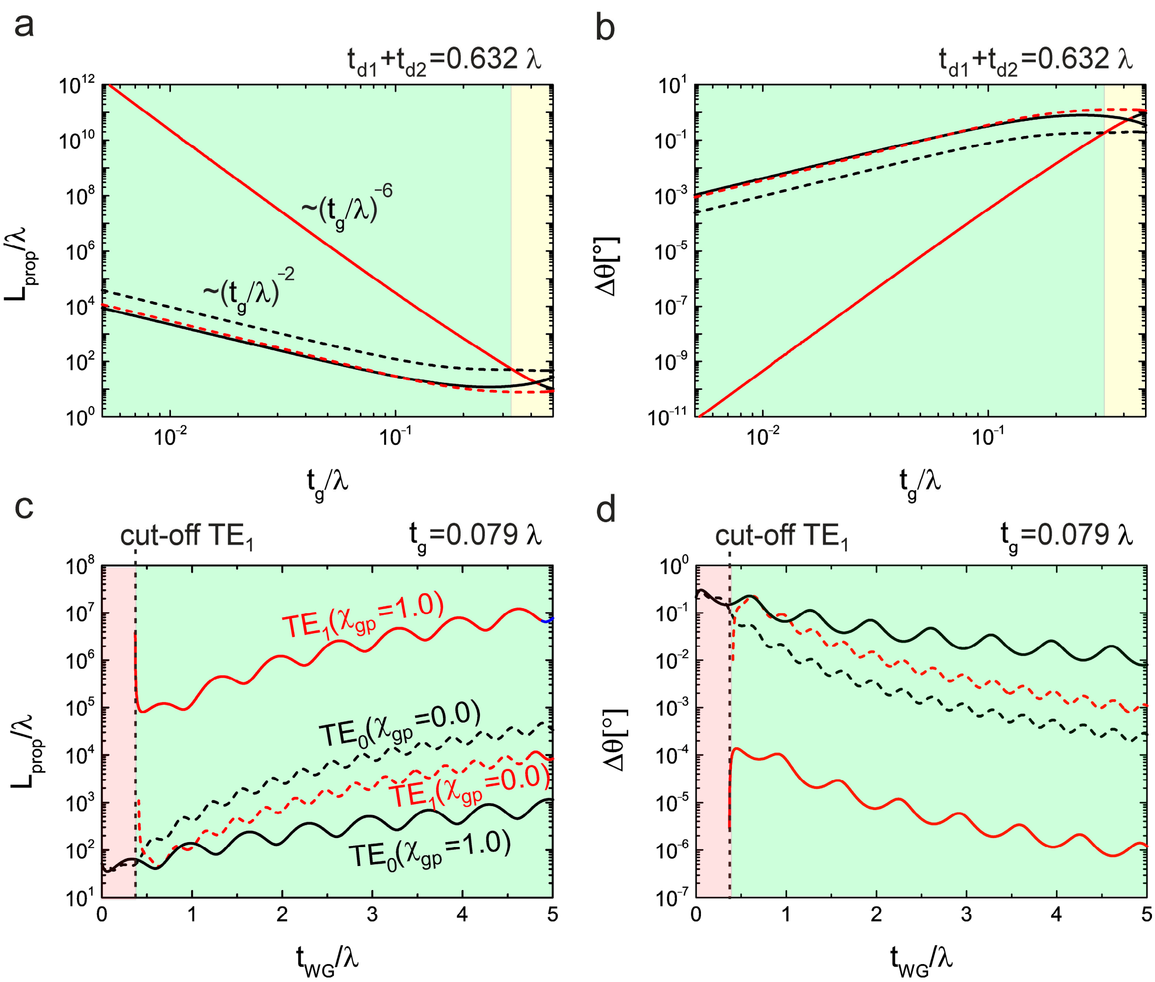

Figure 4. (**a**) The normalized propagation length L_{prop}/λ and (**b**) the divergence angle of the TE_0 mode (black) and TE_1 mode (red) with variation in the normalized grating thickness t_g/λ for $\chi_{gp} = 0.0$ (dashed lines) and $\chi_{gp} = 1.0$ (solid lines) and a fixed normalized waveguide grating thickness $t_{d1} + t_{d2} = 0.632\ \lambda$; (**c**,**d**) corresponding plots with variation in the normalized waveguide grating thickness t_{WG}/λ and a fixed normalized grating thickness $t_g = 0.079\ \lambda$.

Figure 5a shows the dispersion relation of the TE_1 mode at $\chi_{gp} = 1.0$ and the TE_0 mode at $\chi_{gp} = 0.0$, with fixed ratios of all other geometry parameters (identical values to the ones in Figures 3 and 4). Remarkably, large values of L_{prop}/λ between 10^4 and 10^6 are observed for the TE_1 mode over a broad spectral range between $\frac{\lambda}{t_{WG}} = 0.9$ and $\frac{\lambda}{t_{WG}} = 2.0$. This behavior occurs due to the symmetry of the waveguide grating, which enforces the node of the TE_1 mode to remain at the center plane of the waveguide grating. Therefore, regardless of the wavelength, an equivalent situation as discussed in Figure 3 is apparent when $\frac{\lambda}{t_{WG}}$ is below the cutoff of the TE_1 mode.

In comparison, the TE_0 mode exhibits values of L_{prop}/λ between 10^2 and 10^3 for all values of $\frac{\lambda}{t_{WG}}$.

For an asymmetric geometry ($\chi_{gp} \neq 1.0$, $\chi_n \neq 1.0$), L_{prop}/λ shows a maximum of around 10^5 at a distinct value of $\frac{\lambda}{t_{WG}} = 0.96$ (Figure 5b) for the TE_1 mode. This maximum occurs since the position of the node of $Re(E_y)$ shifts through the waveguide grating with respect to the z-direction as a function of $\frac{\lambda}{t_{WG}}$, and the largest value of L_{prop}/λ is observed when FF is minimized.

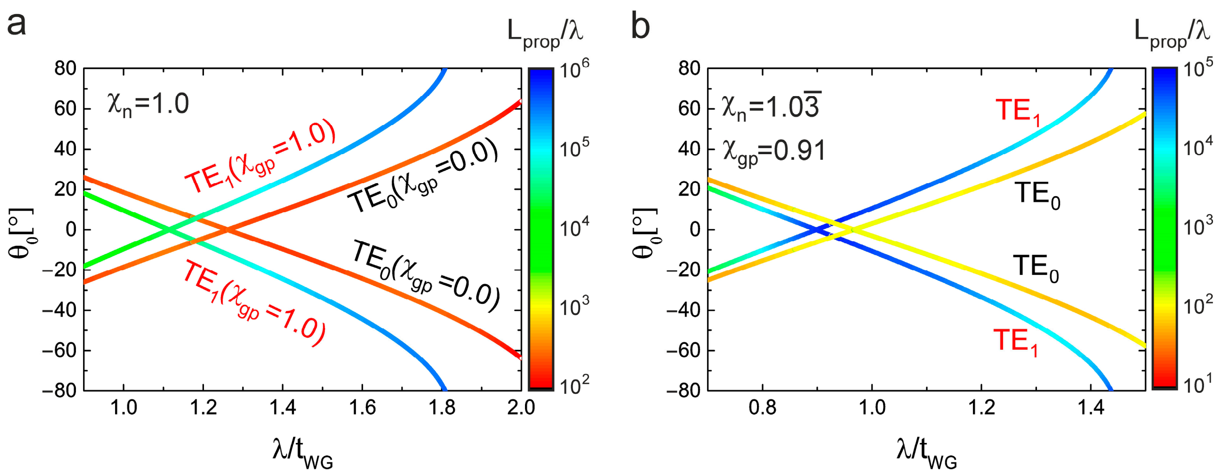

Figure 5. (**a**) The dispersion relations and normalized propagation lengths of the TE_0 mode for $\chi_{gp} = 0.0$ and the TE_1 mode for $\chi_{gp} = 1.0$ under fixed ratios of all geometry parameters as used in Figure 3 (only the wavelength is varied with respect to the geometry) and $\chi_n = 1$; (**b**) dispersion relations and normalized propagation lengths for an asymmetric geometry with $\chi_{gp} = 0.91$, $\chi_n = 1.0\overline{3}$ for both the TE_0 mode and TE_1 mode with $\frac{t_g}{t_{d1}+t_{d2}} = 0.045$.

2.4. Sensitivity to Asymmetric Refractive Index Changes

In the last part of this study, we analyze the sensitivity of the waveguide grating with respect to an asymmetric change in the refractive index at $\chi_{gp} = 1.0$. Such an asymmetric change in the refractive index means that n_{d1} is varied, and n_{d2} remains fixed at a value of 1.5. As a side note, variations in both n_{d1} and n_{d2} at $\chi_n = 1.0$ show almost no sensitivity for the TE_1 mode for any symmetric geometry, as FF is always minimized.

For this exemplary case, the grating thickness was chosen to be $t_g = 1.5 \times 10^{-3}\ \lambda$, whereby all other remaining geometry parameters were chosen to be the same as in Figures 3 and 4.

The following two simulation observations are of interest in order to investigate the sensitivity of the waveguide grating:

(1) For small changes of the refractive index, the figure of merit

$$FoM(n_{d1}) = \frac{1}{L_{prop}(n_{d1})}\frac{\partial L_{prop}(n_{d1})}{\partial n_{d1}}$$

provides a measure for the sensitivity.

(2) For more practical considerations, the refractive index is commonly switched between two distinct values, with a difference of Δn. The sensitivity can be defined by

$$S_{\Delta n} = \frac{L_{prop}(n_{d1} + \Delta n)}{L_{prop}(n_{d1})}$$

Figure 6 shows both L_{prop}/λ and the corresponding FoM, as well as $S_{\Delta n}$ as a function of n_{d1} for the TE_0 mode and the TE_1 mode. Similar to the variation in χ_{gp} in Figures 3–5, the TE_1 mode exhibits high values of L_{prop}/λ around 10^{12} of when χ_n approaches 1.0. Most strikingly, L_{prop}/λ strongly varies with changing values of n_{d1} (Figure 6a). In comparison, the TE_0 mode exhibits nearly constant values of L_{prop}/λ around 10^3. The FoM of the TE_1 mode reaches values of up to 2×10^4, whereas the maximum FoM of the TE_0 mode in the displayed range is 5.6 (Figure 6b). The reason for this large FoM for the TE_1 lies in a strong decrease in L_{prop}/λ consequent to symmetry breaking. Concerning $S_{\Delta n}$ (Figure 6c), for a value of $\Delta n = 1 \times 10^{-4}$ (e.g., in the Pockels effect [18,19]), the values of $S_{\Delta n}$ are close to 1 for the TE_0 mode.

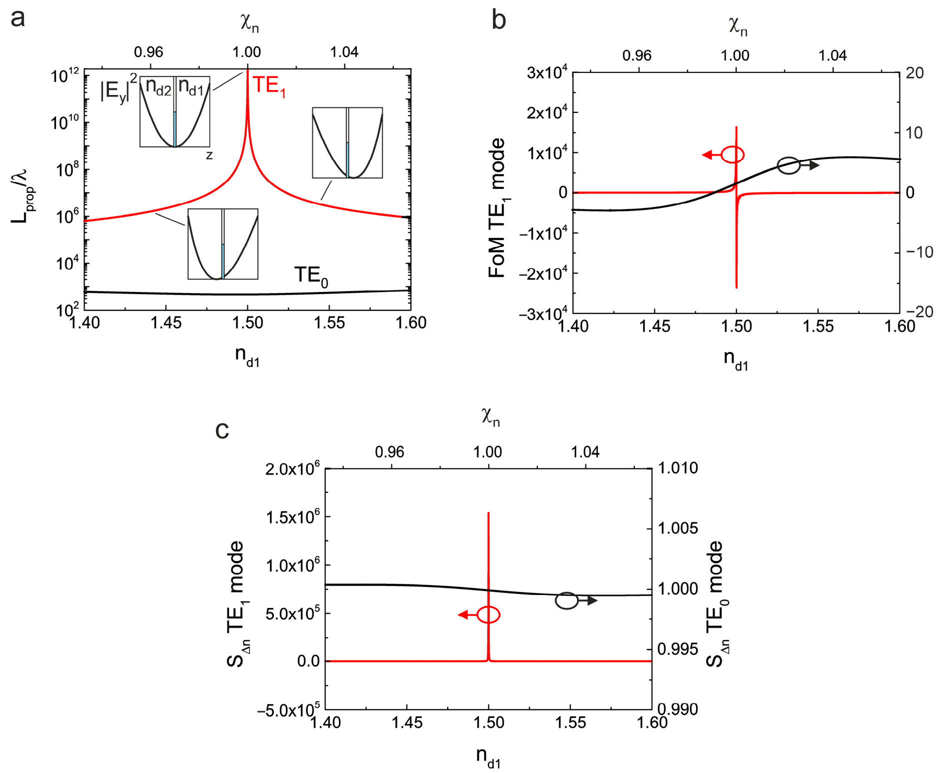

Figure 6. (**a**) The normalized propagation length, (**b**) FoM, and (**c**) $S_{\Delta n}$ of a waveguide grating with $t_g = 1.5 \times 10^{-3}\ \lambda$ and otherwise identical parameters to the ones in Figures 3 and 4 with asymmetric refractive index changes (n_{d1} is varied, and n_{d2} is fixed at a value of 1.5).

However, for the TE_1 mode, it can be observed that $S_{\Delta n}$ exhibits a maximum at $\chi_n = 1.0$, with a substantially higher value of around 1.5×10^6, in comparison to the TE_0 mode. Although fully bound modes ($L_{prop} \to \infty$) cannot be reached, as the filling factor cannot be set to zero, the TE_1 mode allows obtaining much higher propagation lengths and sensitivities with respect to asymmetric refractive index changes than the TE_0 mode using the same geometry. In comparison, reports in the literature regarding the sensitivity of the propagation length with respect to refractive index sensitivity are around $FoM \approx 3$ and $S_{\Delta n} \approx 1.005$ for $\Delta n = 1 \times 10^{-4}$ [21,22].

3. Conclusions

The results presented in this study show a way to drastically increase both the propagation length and sensitivity of waveguide grating by using the TE_1 mode, as long as the grating thickness is small, compared with the waveguide grating thickness. As all results were obtained with the help of an exemplary set of waveguide grating geometries, further optimizations for specific applications such as different refractive indices and grating shapes should be considered in future studies. Nonetheless, as the increased propagation length and sensitivity result from symmetrical conditions, the concept at hand can be applied to a broad range of geometry parameters and wavelengths in general. Control over the propagation length cannot be provided only by changing the refractive index but also by breaking the geometric symmetry of the waveguide grating, e.g., by thermomechanical effects. To be sure, this property also implies the necessity of the accurate control of thickness homogeneity. From the practical point of view, symmetric and homogeneous waveguide gratings can be approached by lamination [29] and are, therefore, in principle, accessible with precise standard fabrication techniques such as roll-to-roll coating [30] in combination with lithography methods [31,32]. Thus, we anticipate this concept to be suited for large-area applications requiring control of the propagation length and divergence angle over many orders of magnitude or sensitivity to environmental changes. Obvious applications are spatially resolved refractive index sensors and light modulators.

4. Methods

All simulations in this research were conducted using rigorous coupled-wave analysis (RCWA) [28]. To ensure the stability of the simulation, we checked both the convergence of the simulated values as well as the conservation of energy (see the Supporting Information). Naturally, as the presented data were calculated for TE polarization, fast convergence and large stability were already obtained for a low number of Fourier orders.

Supplementary Materials: The following supporting information can be downloaded at: https://www.mdpi.com/article/10.3390/opt3010008/s1, Figures S1: (a,b) The convergence of L_{prop} as a function of the number of Fourier orders at the smallest ($t_g = 1.5{\cdot}10^{-3}\ \lambda$) and thickest grating layer thicknesses $t_g = 0.4{\cdot}10^{-4}\ \lambda$; (c) energy conservation for various grating thicknesses at 15 Fourier orders. For all values, the energy is conserved, confirming the stability of the simulation. Figure S2: (a,b) L_{prop}/λ and $\Delta\theta$ as a function of t_g/λ for a waveguide grating with a blaze grating geometry and otherwise identical parameters as in Figure 3. The black and red dots indicate the TE_0 and TE_1 modes for $\chi_{gp} = 1.0$, respectively. Figure S3: (a,b) L_{prop}/λ and $\Delta\theta$ as functions of t_g/λ for a waveguide grating with a lossy grating ($n_{g1} = n_{d1}$ and $n_{g2} = 0.06 + 4.24j$) and otherwise identical parameters as in Figure 3. The black and red lines indicate the TE_0 and TE_1 modes for $\chi_{gp} = 1.0$, respectively. Figure S4: (a,b) L_{prop}/λ and $\Delta\theta$ as a function of Λ/λ for a waveguide grating with otherwise identical parameters to the geometry in Figure 3 for $\chi_{gp} = 1.0$.

Author Contributions: The manuscript was written through the contributions of all authors. Conceptualization, M.M. and P.G.; methodology, M.M. and P.G.; software, M.M.; validation, M.M., P.G., A.H. and M.B.; formal analysis, M.M. and P.G.; investigation, M.M. and P.G.; resources, P.G.; data curation, M.M.; writing—original draft preparation, M.M. and P.G.; writing—review and editing, M.M., A.H., M.B. and P.G.; visualization, M.M.; supervision, P.G.; project administration, P.G.; funding acquisition, P.G. All authors have read and agreed to the published version of the manuscript.

Funding: This research was funded by the European Research Council (ERC), grant number 637367 and the Federal Ministry of Education and Research, contract number 13N15390.

Institutional Review Board Statement: Not applicable.

Informed Consent Statement: Not applicable.

Data Availability Statement: The data in this study are available on request from the corresponding author. Supporting data are available in the Supporting Information.

Acknowledgments: For financial support, this project received funding from the European Research Council (ERC) under the European Union's Horizon 2020 research and innovation program (Grant Agreement No. 637367), as well as the Federal Ministry of Education and Research (Photonics Research Germany funding program, Contract No. 13N15390).

Conflicts of Interest: The authors declare no conflict of interest.

References

1. Belt, M.; Davenport, M.L.; Bowers, J.E.; Blumenthal, D.J. Ultra-low-loss Ta_2O_5-core/SiO_2-clad planar waveguides on Si substrates. *Optica* **2017**, *4*, 532–536. [CrossRef]
2. Yeniay, A.; Gao, R.; Takayama, K.; Gao, R.; Garito, A.F. Ultra-low-loss polymer waveguides. *J. Light. Technol.* **2004**, *22*, 154–158. [CrossRef]
3. Rickman, A.; Reed, G.T.; Weiss, B.L.; Namavar, F. Low-loss planar optical waveguides fabricated in SIMOX material. *IEEE Photonics Technol. Lett.* **1992**, *4*, 633–635. [CrossRef]
4. Yang, L.; Saavedra, S.S.; Armstrong, N.R.; Hayes, J. Fabrication and Characterization of Low-Loss, Sol-Gel Planar Waveguides. *Anal. Chem.* **1994**, *66*, 1254–1263. [CrossRef]
5. Ura, S.; Inoue, J.; Kintaka, K.; Awatsuji, Y. Proposal of small-aperture guided-mode resonance filter. In Proceedings of the 2011 13th International Conference on Transparent Optical Networks, Stockholm, Sweden, 26–30 June 2011; pp. 1–4.
6. Wang, S.S.; Magnusson, R. Design of waveguide-grating filters with symmetrical line shapes and low sidebands. *Opt. Lett.* **1994**, *19*, 919–921. [CrossRef]

7. Kintaka, K.; Majima, T.; Inoue, J.; Hatanaka, K.; Nishii, J.; Ura, S. Cavity-resonator-integrated guided-mode resonance filter for aperture miniaturization. *Opt. Express* **2012**, *20*, 1444–1449. [CrossRef]
8. Thurman, S.T.; Morris, G.M. Controlling the spectral response in guided-mode resonance filter design. *Appl. Opt.* **2003**, *42*, 3225–3233. [CrossRef]
9. Wang, S.S.; Magnusson, R. Multilayer waveguide-grating filters. *Appl. Opt.* **1995**, *34*, 2414–2420. [CrossRef]
10. Flanders, D.C.; Kogelnik, H.; Schmidt, R.V.; Shank, C.V. Grating filters for thin-film optical waveguides. *Appl. Phys. Lett.* **1974**, *24*, 194–196. [CrossRef]
11. Kehl, F.; Follonier, S. Self-referenced waveguide grating sensor. *Opt. Lett.* **2016**, *41*, 1447–1450. [CrossRef]
12. Song, F.; Xiao, J.; Xie, A.J.; Seo, S.-W. A polymer waveguide grating sensor integrated with a thin-film photodetector. *J. Opt.* **2013**, *16*, 15503. [CrossRef] [PubMed]
13. Zaytseva, N.; Miller, W.; Goral, V.; Hepburn, J.; Fang, Y. Microfluidic resonant waveguide grating biosensor system for whole cell sensing. *Appl. Phys. Lett.* **2011**, *98*, 163703. [CrossRef]
14. Ferrie, A.M.; Wu, Q.; Fang, Y. Resonant waveguide grating imager for live cell sensing. *Appl. Phys. Lett.* **2010**, *97*, 223704. [CrossRef] [PubMed]
15. Nellen, P.M.; Tiefenthaler, K.; Lukosz, W. Integrated optical input grating couplers as biochemical sensors. *Sens. Actuators* **1988**, *15*, 285–295. [CrossRef]
16. Clerc, D.; Lukosz, W. Integrated optical output grating coupler as biochemical sensor. *Sens. Actuators B Chem.* **1994**, *19*, 581–586. [CrossRef]
17. Vörös, J.; Ramsden, J.J.; Csúcs, G.; Szendrő, I.; De Paul, S.M.; Textor, M.; Spencer, N.D. Optical grating coupler biosensors. *Biomaterials* **2002**, *23*, 3699–3710. [CrossRef]
18. Kumada, A.; Hidaka, K. Directly High-Voltage Measuring System Based on Pockels Effect. *IEEE Trans. Power Deliv.* **2013**, *28*, 1306–1313. [CrossRef]
19. Gervais, F.; Fonseca, V. Lithium Tantalate ($LiTaO_3$). In *Handbook of Optical Constants of Solids*; Academic Press: Cambridge, MA, USA, 1997; pp. 777–805. ISBN 978-0-12-544415-6.
20. Weis, R.S.; Gaylord, T.K. Lithium niobate: Summary of physical properties and crystal structure. *Appl. Phys. A* **1985**, *37*, 191–203. [CrossRef]
21. Wang, Q.; Zhang, D.; Huang, Y.; Ni, Z.; Chen, J.; Zhong, Y.; Zhuang, S. Type of tunable guided-mode resonance filter based on electro-optic characteristic of polymer-dispersed liquid crystal. *Opt. Lett.* **2010**, *35*, 1236–1238. [CrossRef]
22. Forouzmand, A.; Mosallaei, H. Electro-optical Amplitude and Phase Modulators Based on Tunable Guided-Mode Resonance Effect. *ACS Photonics* **2019**, *6*, 2860–2869. [CrossRef]
23. Görrn, P. Method for Concentrating Light and Light Concentrator. U.S. Patent 10,558,027, 2 July 2014.
24. Rabe, T.; Görrn, P.; Lehnhardt, M.; Tilgner, M.; Riedl, T.; Kowalsky, W. Highly sensitive determination of the polaron-induced optical absorption of organic charge-transport materials. *Phys. Rev. Lett.* **2009**, *102*, 137401. [PubMed]
25. Görrn, P.; Rabe, T.; Riedl, T.; Kowalsky, W. Loss reduction in fully contacted organic laser waveguides using TE 2 modes. *Appl. Phys. Lett.* **2007**, *91*, 041113.
26. Ura, S.; Yamada, K.; Lee, K.J.; Kintaka, K.; Inoue, J.; Magnusson, R. Guided-mode resonances in two-story waveguides. In Proceedings of the 2017 19th International Conference on Transparent Optical Networks (ICTON), Girona, Spain, 2–6 July 2017; pp. 1–4.
27. Görrn, P. Waveguide, Method of Projecting Light from a Waveguide, and Display. U.S. Patent 10,739,623, 20 October 2017.
28. Tamir, T.; Zhang, S. Modal transmission-line theory of multilayered grating structures. *J. Light. Technol.* **1996**, *14*, 914–927. [CrossRef]
29. Meudt, M.; Bogiadzi, C.; Wrobel, K.; Görrn, P. Hybrid Photonic–Plasmonic Bound States in Continuum for Enhanced Light Manipulation. *Adv. Opt. Mater.* **2020**, *8*, 2000898. [CrossRef]
30. Park, J.; Shin, K.; Lee, C. Roll-to-Roll Coating Technology and Its Applications: A Review. *Int. J. Precis. Eng. Manuf.* **2016**, *17*, 537–550. [CrossRef]
31. Guo, L.J. Nanoimprint Lithography: Methods and Material Requirements. *Adv. Mater.* **2007**, *19*, 495–513. [CrossRef]
32. Lu, C.; Lipson, R.H. Interference lithography: A powerful tool for fabricating periodic structures. *Laser Photon. Rev.* **2010**, *4*, 568–580. [CrossRef]